Investigation of kinematic analysis in the Tanumah area, Arabian shield, Saudi Arabia

Osama M. K. Kassem[1, 2]

1- SGSRC, Department of Geologyand Geophysics, Science faculty, King Saud University, P.O. Box 2455, Riyadh 11451, Kingdom of Saudi Arabia.
2- Department of Geology, National Research Center, Al-Behoos str., 12622 Dokki, Cairo, Egypt.

* Corresponding Author: kassemo1@yahoo.com

Received: 22 November 2014 / Accepted: 23 January 2015 / Published online: 27 January 2015

Abstract

New structural, metamorphic, finite strain and kinematic vorticity data for granitic gneiss and metavolcano-sedimentary rocks of theTanumaharea in the Arabian shield in Saudi Arabia reveal a history of deformation reflecting different tectonic regimes. Kinematic analysis shows their relationship to the nappe contacts between the granitic gneiss and metavolcano-sedimentary rocks and explains the nature of the subhorizontal foliation typical for theTanumaharea. The vorticity analysis of porphyroclasts was determined in high temperature mylonites. The kinematic vorticity number for the mylonitic granitic and metavolcano-sedimentary samples in the Tanumaharea range from 0.60 to 0.90, and together with the strain data suggest deviations from simple shear. The data indicate oblate strain symmetry (flattening) in the Tanumah area and the strain magnitudes do not increase towards the tectonic contacts. It is suggested that the accumulation of finite strain was not associated with any significant volume change. The penetrative subhorizontal foliation is subparallel to the tectonic contacts with the overlying nappes and foliation was formed during nappe thrusting and intrusion of granite rocks under semi-brittle to ductile deformation in the Tanumah area. It can be concluded that the accumulation of ductile strain during thrusting was not by simple shear and involved a component of vertical shortening, which caused the subhorizontal foliation in Tanumaharea and adjacent units.

Keywords: Kinematic Analysis, Deformation, Tanumah Area, Arabian Shield, Saudi Arabia.

1–Introduction

The Arabian shield is interpreted as a collage of amalgamated tectono-stratigraphic terranes (Fig. 1). Many authors show that terrane analysis is based on apparent isotopic, structural, geochronologic, and lithostratigraphic differences that divide the shield into small to large crustal blocks bounded by shear zones, some of which represent original sutures, others of which are younger transcurrent faults (Johnson and Woldehaimanot, 2003; Stoeser and Camp, 1985; Stern, 1994; Genna et al., 2002; Nehlig et al., 2002; Stoeser and Frost, 2006). The terranes are made up of the earliest formed rocks in any given part of the shield and mostly originated in a juvenile Neoproterozoic ocean.

As a result of ongoing subduction and the consumption of intervening oceanic crust, the terranes in the shield converged, amalgamated, and sutured, in an orogenic process characterized by metamorphism, deformation, and syntectonic intrusion. On the basis of dating

the metamorphic and intrusive events in the terranes and along the suture zones between the terranes, it is evident that orogeny was not synchronous across the shield. The oldest amalgamation events are along the Bi'r Umq suture (780–760 Ma) (Hargrove, 2006); the youngest are along the Al Amar suture (Doebrich, et al., 2007). With the exception of the Ad Dawadimi, Ar Rayn, and Ha'il terranes, the terranes appear to be composite, containing smaller crustal units that record internal amalgamation histories. The Ad Dawadimi terrane is uniquely sedimentary in origin, and the Afif terrane contains a microplate of Paleoproterozoic continental crust (the Khida subterrane).

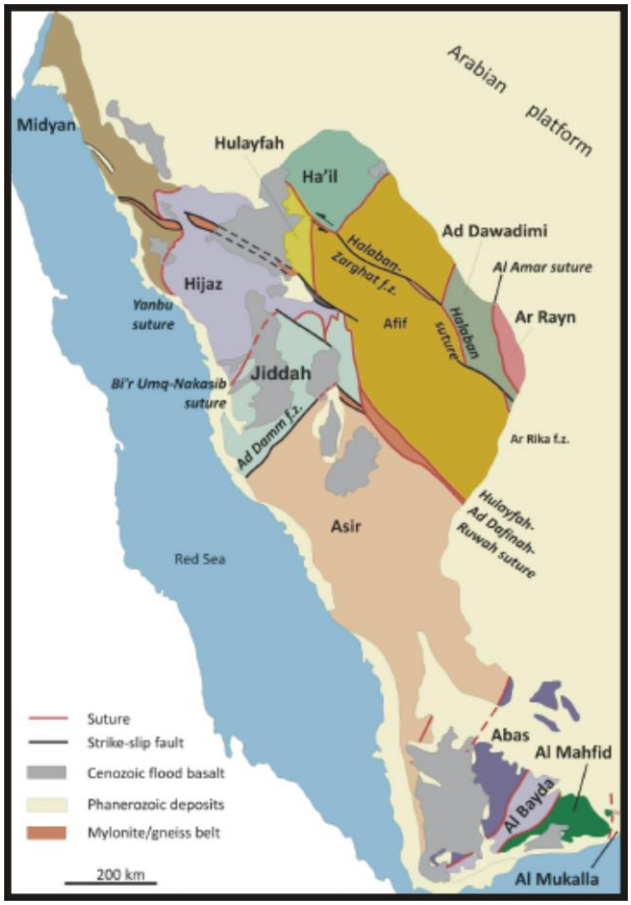

Figure 1) Tectonostratigraphic terranes in the Arabian shield [modified after Stoeser, and Camp (1985)].

The suture zones are characteristically linear belts of obducted ophiolitic material, commonly serpentinized peridotite and gabbro, intruded by syntectonic granite–granodiorite gneiss. Younger rocks in the shield consist of volcanic and sedimentary assemblages deposited in post-amalgamation basins and granitic rocks emplaced in a vast number of late-to-post-tectonic intrusions. The post-amalgamation basins are unconformable on the amalgamated terranes or overlap terrane boundaries (or sutures), and the late-to-post-tectonic intrusions commonly intrude the suture zones and "stitch" terranes together (Fig. 1).

Tanumah is located on the highlands of Asir Mountains, south-west in Saudi Arabia at 18°58' N, 42°06' E and about 1920 m above sea level. It is about 110 km north of Abha near (600 m) the Taif-Abha main road. It is located in the highland region, the Tanumah area consists of metavolcanics, meta-andesite, metasedimentary, biotite quartz diorite, gneissic quartz diorite, tonalite and granodiorite and granite rocks.

Many authors have tried to understand the kinematics, deformation conditions, and tectonic significance of brittle-ductile shear zones. General techniques have been developed to quantitatively evaluate both strain and vorticity in deformed rocks (Passchier, 1987; Passchier and Urai, 1988; Simpson and De Paor 1993; Tikoff and Teyssier, 1994; Ring and Kassem, 2007; Kassem and Abd El Rahim, 2010; Kassem, 2011; Kassem, 2012; Kassem et al., 2012; Al-Saleh and Kassem, 2012; Kassem, 2014a). However, many studies have quantified the strain and vorticity path in naturally deformed rocks] (c.f. Wallis, 1992; Simpson and De Paor, 1997). In the study of deformation in ductile shear zones, it is commonly assumed that strain has accumulated by progressive simple shear] (Passchier 1987; Simpson and De Paor, 1993). However, other types of steady-state progressive deformation are also possible. For deformation with no volume change, three types of plane-strain steady deformation can be defined: pure shear, simple shear and general non-coaxial shear that is intermediate between the other two (Ghosh and Ramberg, 1976; Passchier, 1987; Passchier and Urai, 1988; Kassem and Ring, 2004; Ring and Kassem,

2007). For these types of deformation, the differences in the type of associated flow can be described in terms of the degree of non-coaxiality (Malvern, 1969; Elliott, 1972; Means et al., 1980; Lister and Williams, 1983; Passchier, 1986). The degree of non-coaxiality of deformation gives a measure of the relative contribution of rotation to stretching during deformation. In the analysis of finite deformation, the degree of non-coaxiality is commonly expressed by the mean kinematic vorticity number, Wm (Passchier, 1987).

This study presents an investigation into the effect of different combinations of pure and simple shears, matrix rheology, object aspect ratio and resultant flow perturbation on the development of shape-preferred orientation of a population of rigid objects during progressive deformation for the mylonitized granite in the northern thrust in Tanumah area to explain the stage of orogeny during nappes form. In addition, this work aims to detection of the orientation of rigid objects during progressive deformation.

2– Geological setting

The Tanumah area is located in the Asir terrane, which consists of metamorphosed volcanic, sedimentary and plutonic rocks strongly deformed by isoclinal, north-trending folds and north-trending ductile shear zones with steeply dips (Fig. 2). The Asir terrane evolved by the assembly of ocean-plateau, spreading center and island-arc deposits that crop out in two broad north-trending structural belts referred to as the An Nimas (840-810 Ma) and Tarib (>720 Ma) arcs (Stoeser and Stacey, 1988).

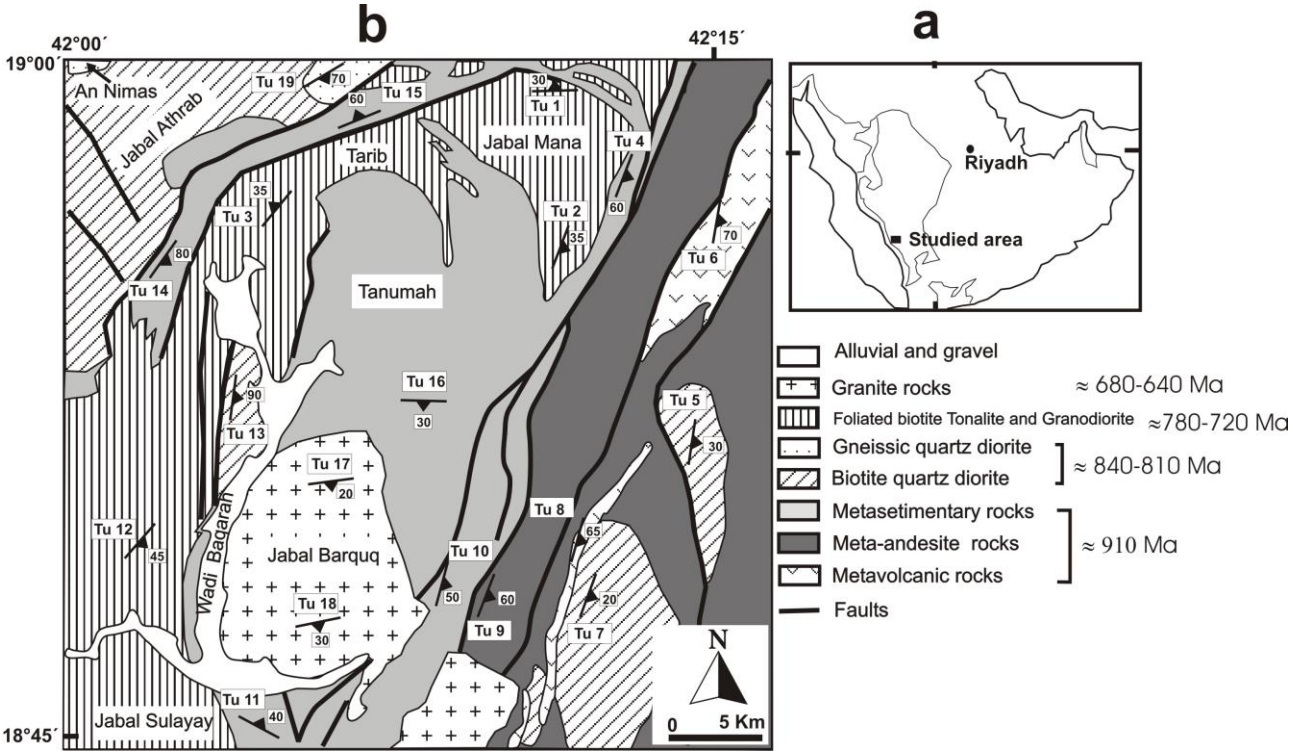

Figure 2a) Location of studied area. b) Geological sketch map of Tanumah area and showing samples locations show strike and plunging directions (All information about age rock units in legend map after Stoeser and Stacey ,1988).

The arc deposits were intruded by large amounts of arc-related calc-alkaline diorite, trondhjemite, tonalite and granodiorite, and by two phases of syntectonic orthogneiss, the younger of which is dated about 680-640 Ma (Stoeser and Stacey, 1988). It is provisionally estimated that the terrane was assembled sometime between 720-680 Ma, after the formation of the Tarib arc and prior to emplacement of the 680-640 Ma gneisses.

Metavolcanic rocks were intruded by dioritic rocks and are about 912 Ma (Greenwood, 1979). Metavolcanic rocks include volcanic greywacke, slate, chert, bedded tuff and interbeds of volcanic flow rock. The rocks are weakly to moderately foliated and are metamorphosed to greenschist facies. They have Schistosity dips steeply east or west (Fig. 2). This north-trending grain was distorted during emplacement of the granodiorite and granite suite with the steep dips. Stoeser, and Stacey, (1988) explain that near intrusive contacts, amphibolites-grade metamorphic hornfelsed rocks contain isoclinally folded schistosity.

Meta-andesite rocks occur interbedded with the metavolcanic rocks and bounded by a major fault that separated metasedimentary (Fig. 2). The remnant faults are bounded of the metavolcanic rocks to meta-andesite in the area. The lithologies of metasedimentary interbeds in the meta-andesite rocks are similar to those metavolcanic. The proportion of metavolcanic and metasedimentary rocks varies along and across the belt. These rocks are elongated grain and parallel to the regional structural. The meta-andesite rocks are regionally metamorphosed to the greenschist facies. They are transposed along ductile faults and the intrusion of plutonic domes.

Metasedimentary rocks consist of phyllite, slate, graywake and subordinate quartzite (Fig. 2). The metasedimentary rocks are folded and contain a strong schistosity. Proterozic intrusive rocks range in age from about 620 to 840 Ma (Stoeser and Stacey, 1988). Diorite suite forms part of the southern extension of the Nimas batholith (Greenwood 1979; Greenwood, et al., 1982) and composed of rocks emplaced between 840 and 800 Ma. They are the largest discrete dioritic batholith in the southern Arabian Shield. The batholith is a composite of dioritic rocks that were emplaced in two or more phases (Greenwood et al., 1982). These rocks occur as fault bounded outcrops and intrude meta-andesites. These rocks are gneissic, a result of post-emplacement metamorphism and tectonism during the diapiric rise of the adjacent biotite tonalite and granodiorite. The intrusion of biotite tonalite and granodiorite gneisses appears to have domed and metasomatically altered the dioritic rocks. The altered diorite and quartz diorite contain sparse metasomatic microcline and muscovite.

Tonalite and granodiorite suite is composed of gneissic rocks emplaced between 780 and 760 Ma (Fleck et al., 1980). They intrude the metasedimentary rocks near wadi Baqarah (Prinz, 1975; Greenwood, 1979) (Fig. 2). The suite was emplaced in two or more phases between approximately 780 and 760 Ma. The tonalite and granodiorite are similar; both are gneissic and contain muscovite, biotite and garnet. The gneiss near Jabal Mana has a strong foliation parallel with its contacts and is separated by metasedimentary rocks (Fig. 2). The gneiss shows injection contact with the metasedimentary rocks in which kyanite is present. The granodiorite is strongly foliated; it is locally gneissic near its contacts. It also contains many inclusions of metasedimentary rocks. In the near Jabal Mana, the fault was located between metasedimentary rocks and the Tonalite and granodiorite rocks. This fault coincides with a sharp break in metamorphic character. The boundary is transitional which depends on the juxtaposed rocks and a sharp transition occurs where metasedimentary rocks are juxtaposed to meta-andesite rocks (Fig. 2).

Granite suite composed of granitic rocks emplaced between 670 and 620 Ma (Felck et al., 1980; Stoeser et al., 1984). It crops out as intrusion in Jabal Barquq. The rocks are light gray to white, coarse to very coarse grained and massive. It consists of quartz, microcline, plagioclase, and accessory muscovite, biotite and garnet (Fig. 2).

3–Methodology

Nineteen samples were collected from the granitic gneisses and metavolcano-sedimentary succession rocks in the Tanumaharea. For the strain measurements, the R_f/φ and Fry methods were used on feldspar, quartz and some mafic minerals from two metavolcanic, one meta-andesite, six metasedimentary, four diorite suite, four tonalite-granodiorite and two granite rocks (Fig. 2). The Fry method was applied to all samples to compare the results with those obtained by the R_f/φ method. The feldspar and mafic grains were marked and scanned. The traced outlines were then digitised. A least squares best-fit ellipse was calculated for each marker outline as well as its relative position and orientation.

R_f/ϕ Method: In order to show that the strain analysis with the R_f/ϕ method would have meaningful results, it is imperative to demonstrate that the measured objects deformed homogeneously together with their matrix. The R_f/ϕ technique is, in fact, based on calculating the theoretical distribution of final ellipticities and orientations that result from imposing different strains on objects that have a known initial ellipticity and orientation. The finial ellipticity R_f and the orientation ϕ of a deformed object depend on the initial ellipticity R_i, on the initial orientation θ of the undeformed object, and on the ellipticity R_s of the imposed strain ellipse. In order to evaluate the initial feldspar fabric, the strained distributions of the feldspar grains were undeformed using the procedure (program THETA) described by Peach and Lisle (1979). The method superimposes a coaxial strain having its long axis at right angles to the preferred orientation on the R_f/ϕ distribution. The magnitude of this superimposed strain is incremented and after each step the randomness of the resultant undeformed orientation of the markers is calculated. If no initial fabric is present, the reciprocal finite strain value can be determined from the strain necessary to bring about the most uniform particle distribution.

Fry method: The Fry method is useful for determining the strain ellipse from a large number of points. In essence, it involves plotting the length and orientation of a large number of center-to-center lines relative to a single reference point. Fry (1979) proposed the all object-object separations method, where the relative positions of adjacent grains are directly plotted by sequentially putting the origin of an overlay on each centre and recording the position of adjacent centres as points. In many aggregates, these points define an elliptical void and parallel ring of high point-density around the origin of the overlay. These ellipses will equal the finite-strain ellipse for homogeneously deformed populations of originally statistically uniform centres. The advantage of the Fry method is that it provides a graphical solution to the centre-to-centre method, which is both rapid and accurate, and that one sees from the developing graph when enough data have been plotted to provide an answer of sufficient accuracy for the investigation in hand. This technique provides an excellent practical method for finding the best-fit solution to the strain ellipse.

Kinematic vorticity number (W_m): Methods for estimation of kinematic vorticity number (W_m) have been made using rotated rigid objects (Passchier, 1987; Cowan, 1990; Ring, 1998), deformed vein sets (Passchier, 1990; Wallis, 1992), the stretch and rotation of material lines (Passchier and Urai, 1988) and curved fibres around quartz and feldspar objects (Ring and Brandon, 1999; Ring et al., 2001). For quantifying the degree of non-coaxiality from rotated rigid objects, the equations governing the rotation of rigid objects in a flowing viscous medium were used (Jeffery, 1922; Ghosh and Ramberg, 1976; Passchier, 1987). As shown by Ghosh and Ramberg (1976), the sense and rate of rotation of a particle depend on its orientation, axial ratio (R) and the ratio between the elongation in the shear plane and shear strain. For W_m=1, i.e. simple shear, all particles

which behave as active markers with R≥1 will rotate freely as the shear strain increases and the rate of rotation equals the rate of stretching. If W_m is lower than 1, i.e. a component of pure shear accompanies shearing (general or sub-simple shear of Simpson and De Paor, 1993) and the rotation of particles with progressively smaller aspect ratios is subdued (Cowan, 1990). For any flow regime with $W_m<1$, not all rigid particles are free to rotate continuously. Particles with an aspect ratio above a certain critical value, R_c, will rotate until they reach a stable orientation. For aspect ratios less than the critical value, rotation is unrestricted. The value of R_c that divides freely rotating objects from those that have reached a stable orientation is a function of the degree of non-coaxiality:

$$W_m = (R_c^2 - 1) / (R_c^2 + 1)$$ *(Passchier 1987)*

The sample must meet the five main requirements defined by Passchier (1987): (1) reasonably homogeneous deformation on the scale of the sample, (2) significant difference in grain size between the rigid porphyroclasts and the matrix, (3) high finite strain to rotate objects towards stable-sink positions, (4) porphyroclast shape that is close to orthorhombic, and (5) significant number of porphyroclasts with a range in aspect ratios and orientations.

4– Results of finite-strain analysis

The granitic gneisses and volcano-sedimentary samples are characterized by moderately to highly deformed and oriented clasts for granitic gneisses and deformed metavolcano-sedimentary samples (Fig. 3). The granitic gneisses are metamorphic foliation, emphasized by development of chlorite and sericite, commonly shows the banding and strongly foliation (Fig. 3a). The metavolcano-sedimentary rocks varieties may also show distinct centimeter- to decimeter-thick lithological banding parallel to the schistosity (Fig. 3b).

The field orientations and sample locations for finite strain analysis of the metavolcanics and metasedimentary samples in the Tanumah area are shown in Fig. 4 and Table 1. The data indicates that the trends of the long axes of the finite strain ellipsoid (maximum extension direction X-axes) are characterized by WNW - ESE with plunge gently to moderately (Fig. 4a).

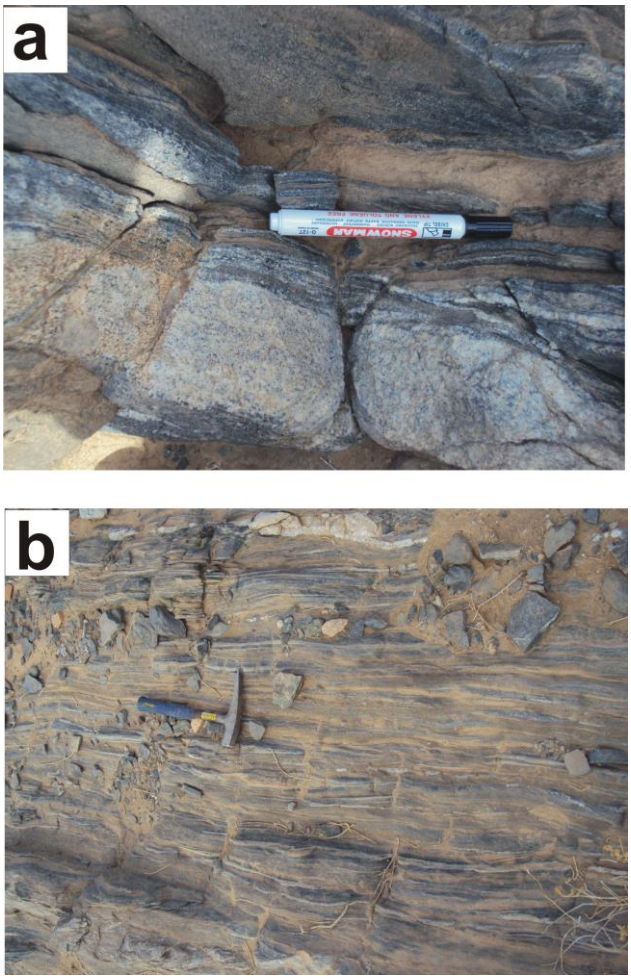

Figure 3) Field photographs of (a) Mylonitic texture in granite gneiss indicating heterogeneous deformation and lithological banding parallel to the gneissosity (Sample Tu 18).b) Metavolcano-sedimentary rocks varieties may also show lithological banding parallel to the schistosity (Sample Tu 14).

In particular, the mean value for the long axes for all units shows along WNW - ESE trend with a plunge of about 29° (Kassem, 2014b), intermediate direction Y-axes display ENE to WSW direction and a moderate angle of plunge (Fig. 4b). The mean for all units has ENE to WSW trend, a dipping plunge about 6°. It shows

a subperpendicular attitude with respect to the X direction (Fig. 4b). The maximum shortening direction (Z) plunges steeply to the WNW-ENE (Fig. 4c). Contouring of all collected data for Z-axes reveals the orientation of the axis is 225°with plunge 60° (see Kassem, 2014b).

Table 1) Direction of finite strain axes and stretches for samples from Tanumah area.

Sample No.	X			Y			Z		
	Trend	Plung	Stretch	Trend	Plung	Stretch	Trend	Plung	Stretch
Tu1	310	15	1.69	215	15	0.93	80	70	0.63
Tu2	330	17	1.66	235	16	1.06	100	65	0.57
Tu3	145	25	1.45	50	17	1.05	290	60	0.66
Tu4	320	30	1.67	60	13	1.04	170	58	0.58
Tu5	122	10	1.21	30	20	1.17	240	67	0.71
Tu6	310	12	1.43	215	30	1.07	60	60	0.65
Tu7	130	30	1.44	35	10	1.03	288	58	0.68
Tu8	325	10	1.29	58	16	1.08	202	71	0.71
Tu9	335	25	1.48	70	13	1.09	180	65	0.62
Tu10	320	20	1.25	60	28	1.10	200	56	0.73
Tu11	100	30	1.47	5	10	1.11	262	58	0.61
Tu12	160	20	1.38	65	15	1.22	300	66	0.59
Tu13	348	20	1.63	90	30	1.09	225	58	0.56
Tu14	350	20	1.8	255	10	1.08	146	66	0.51
Tu15	120	30	1.8	22	12	1.27	273	57	0.44
Tu16	115	30	1.91	20	10	1.07	275	57	0.49
Tu17	330	20	1.4	235	15	1.07	110	60	0.67
Tu18	290	10	1.31	190	30	1.1	40	55	0.69
Tu19	155	10	1.95	60	25	1.26	265	65	0.41
Tensor Average	170	29		70	6		223	60	

The strain data are summarized in Table 1and 2 and shown in a Flinn diagram (Fig. 5) which shows the relative shapes of the strain ellipsoids, i.e. prolate vs oblate. Information on volume strain is needed, to infer strain type, i.e. constrictional vs flattening. However, minor or no volume changes are expected in high grade rocks in which porosities during deformation were probably very small specially for the basement rocks (Ramsay and Huber, 1983; Kassem and Ring, 2004; Kassem, 2008; Kassem and Abd El Rahim 2010; Kassem, 2014b). Kassem and Ring (2004) shows oblate strain symmetry (flattening strain) in the granitic gneisses and metavolcano-sedimentary samples. The K value defines the ratios of the principal strains. Furthermore, the different shapes of ellipsoids are distinguished using the K value.The strain ellipsoids have oblate strain symmetry (Fig. 5). The strain symmetry as expressed by the K value (Flinn 1962; Ramsay and Huber 1983)shows a relationship to tectonic contacts in the Tanumah area (Fig. 5). The K value defines the ratios of the principal strains. In addition, the K values are calculated from R_f/φ method of the granitic gneisses and metavolcano-sedimentary samples are less than 1 and indicate oblate strain (Fig. 5).

Figure 5represents the R_f/φ and Fry strains. As shown in Figure 5, Fry strains are not fundamentally different from R_f/φ strains; the R_f/φ strains are slightly smaller than the Fry strains. Therefore, there was no significant difference in the deformation behaviour between the quartz-mica matrix and the feldspar porphyroclasts and amphibole grains during the accumulation of finite strain. Furthermore, finite strain of different type of rocks is of the same

order of magnitude. The main-phase foliation does not show any differences between the granitic gneisses and metavolcano-sedimentary samples, which also suggest similar deformation behaviour in all types of rocks. R_f/φ strains derived from analysing quartz and feldspar porphyroclasts (feldspar and plagioclase) and some mafic grains (mica and hornblende) are summarized in Table 2.

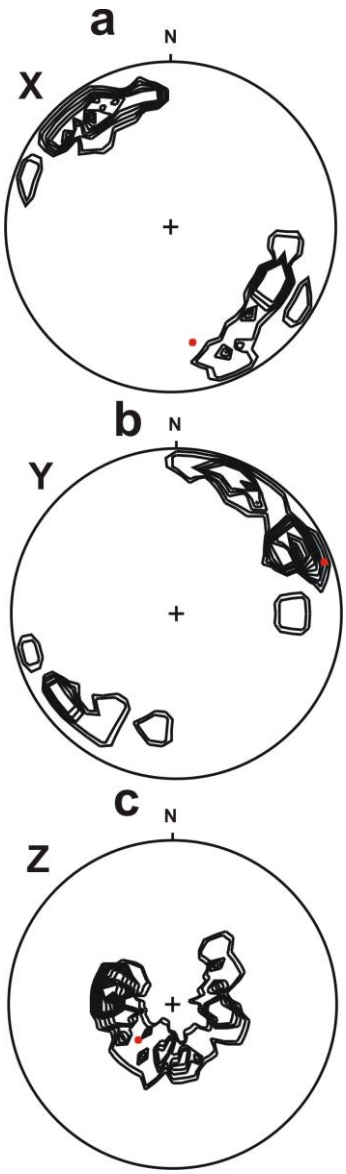

Figure 4) Lower-hemisphere equal-area projections: a) maximum extension direction (X), b) intermediate direction (Y); c) maximum shortening direction (Z). Contours start at 3% and increment every 3%. Red circle in the stereographic projections represent mean values of tensor averages.

Kassem (2014b) shows that the strain ellipsoids have oblate strain symmetry (Fig. 5). The axial ratios in the XZ sections range from 1.70 to 4.80 for the R_f/φ method and from 1.20 to 4.50 for the Fry method that indicate moderate to high deformation (Table 2). In addition, Stretches Sx, Sy and Sz are parallel to the principal axes X, Y, and Z respectively, S_X averages range from 1.21 to 1.95 for the R_f/φ method and from 1.09 to 1.93 for the Fry method. S_Y ranges from 0.93 to 1.26 for the R_f/φ method and from 0.93 to 1.26 for the Fry method, showing contraction and extension in this direction. The stretches in the Z direction (S_Z) range from 0.41 to 0.73, indicating vertical shortening of 27% to 59% for the R_f/φ method. Also, Fry strain data show that S_Z ranges from 0.25 to 0.91, indicating vertical shortening of 9% to 75% (Table 2). The strain data show no significant difference in the deformation behaviour between R_f/φ and Fry methods and the same order of the deformation in all studied rock types is apparent in the field. In this case, Fry strain data support our results for R_f/φ strain data (Kassem, 2014b).

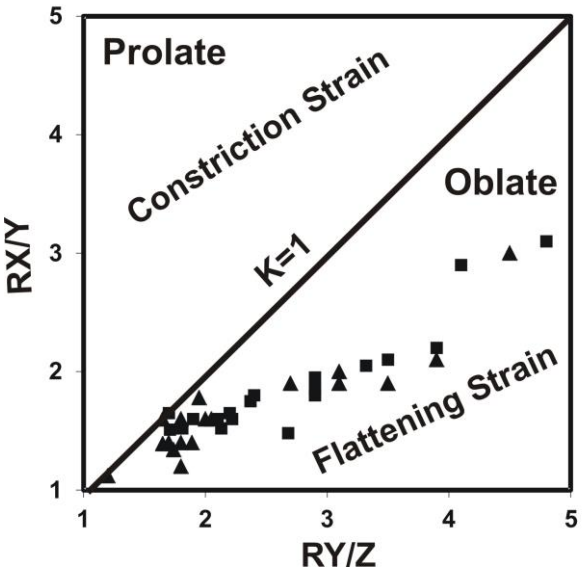

Figure 5) Flinn diagram (Flinn, 1962) showing relative strain or strain symmetry as obtained by the Rf/φ method and the Fry method. Rf/φ strain data are show by black squares and Fry strain data by black triangle from the same samples.

Kassem (2014b) explains that The K value shows a low to moderate value ranging from 0.05 to 0.77 for R_f/φ method and from 0.05 to 0.94 for fry method (Fig. 5). Accordingly, the

strain symmetry is characterized by low to moderate oblate strain symmetries. The strain magnitudes of the different type of samples in the Tanumah area have averages ranging from 0.397 to 1.145, which indicate a heterogeneous deformation (Table 2).

Table 2) Finite strain data and mean kinematic vorticity number for sample from Tanumah area.

Sample No.	Method	Rc	Wm	Rxy	Ryz	Rxz	Stretch			Principal strain ratios	Radius	Strain magnitude
							Sx	Sy	Sz	K	r	Et
Tu1	Rf/PHI	3.15	0.82	1.81	1.48	2.68	1.69	0.93	0.63	0.75	2.29	0.702
	Fry			1.50	1.20	1.80	1.39	0.93	0.77	0.70	1.70	0.425
Tu2	Rf/PHI	3.5	0.85	1.57	1.85	2.90	1.66	1.06	0.57	0.67	2.42	0.756
	Fry			1.21	1.40	1.70	1.27	1.05	0.75	0.54	1.61	0.380
Tu3	Rf/PHI	5	0.92	1.39	1.60	2.22	1.45	1.05	0.66	0.65	1.99	0.567
	Fry			1.29	1.40	1.80	1.32	1.03	0.73	0.71	1.69	0.417
Tu4	Rf/PHI	----	----	1.61	1.80	2.90	1.67	1.04	0.58	0.76	2.41	0.754
	Fry			1.70	1.90	2.70	1.57	1.10	0.58	0.65	2.32	0.712
Tu5	Rf/PHI	2.7	0.76	1.03	1.65	1.70	1.21	1.17	0.71	0.05	1.68	0.422
	Fry			1.03	1.60	1.65	1.19	1.16	0.72	0.05	1.63	0.397
Tu6	Rf/PHI	3.3	0.83	1.33	1.65	2.20	1.43	1.07	0.65	0.51	1.98	0.564
	Fry			1.19	1.39	1.65	1.25	1.05	0.76	0.48	1.58	0.360
Tu7	Rf/PHI	3.2	0.82	1.40	1.52	2.13	1.44	1.03	0.68	0.77	1.92	0.536
	Fry			1.07	1.12	1.20	1.09	1.01	0.91	0.60	1.19	0.130
Tu8	Rf/PHI	----	----	1.19	1.52	1.81	1.29	1.08	0.71	0.37	1.71	0.431
	Fry			1.30	1.34	1.74	1.31	1.01	0.75	0.88	1.64	0.392
Tu9	Rf/PHI	----	----	1.35	1.75	2.37	1.48	1.09	0.62	0.47	2.10	0.619
	Fry			1.35	1.40	1.89	1.37	1.01	0.72	0.88	1.75	0.450
Tu10	Rf/PHI	3.9	0.88	1.13	1.51	1.71	1.25	1.10	0.73	0.26	1.64	0.397
	Fry			1.10	1.78	1.95	1.21	1.18	0.66	0.12	1.88	0.512
Tu11	Rf/PHI	----	----	1.33	1.8	2.4	1.47	1.11	0.61	0.42	2.13	0.631
	Fry			1.28	1.6	2.05	1.38	1.08	0.67	0.47	1.88	0.516
Tu12	Rf/PHI	2.6	0.74	1.62	2.05	3.32	1.75	1.08	0.53	0.59	2.67	0.854
	Fry			1.55	2	3.1	1.69	1.09	0.54	0.55	2.55	0.807
Tu13	Rf/PHI	----	----	1.49	1.95	2.9	1.63	1.09	0.56	0.51	2.44	0.761
	Fry			1.21	1.4	1.7	1.27	1.05	0.75	0.54	1.61	0.380
Tu14	Rf/PHI	----	----	1.67	2.1	3.5	1.8	1.08	0.51	0.61	2.77	0.891
	Fry			1.63	1.9	3.1	1.72	1.05	0.55	0.7	2.53	0.802
Tu15	Rf/PHI	4.9	0.92	1.41	2.9	4.1	1.8	1.27	0.44	0.22	3.31	1.040
	Fry			1.86	2.1	3.9	1.93	1.04	0.5	0.78	2.96	0.964
Tu16	Rf/PHI	----	----	1.77	2.2	3.9	1.91	1.07	0.49	0.64	2.97	0.966
	Fry			1.84	1.9	3.5	1.86	1.01	0.53	0.94	2.74	0.886
Tu17	Rf/PHI	4.3	0.89	1.31	1.6	2.1	1.4	1.07	0.67	0.52	1.91	0.531
	Fry			1.25	1.6	2	1.36	1.09	0.68	0.42	1.85	0.500
Tu18	Rf/PHI	3.1	0.81	1.19	1.6	1.9	1.31	1.1	0.69	0.31	1.79	0.470
	Fry			1.13	1.6	1.8	1.27	1.12	0.7	0.21	1.73	0.440
Tu19	Rf/PHI	5.4	0.93	1.55	3.1	4.8	1.95	1.26	0.41	0.26	3.65	1.145
	Fry			1.5	3	4.5	1.89	1.26	0.25	0.25	3.5	1.101

5– Flow path analysis

Kassem and Ring (2004) showed that finite-strain data from the same type of rocks in conjunction with the chemical data (XRF analysis) indicate flattening strain type, which suggests that deformation deviated from simple shear. To quantify the degree of non-coaxiality, a flow-path analysis was carried out by using rotated rigid objects (Passchier, 1987). In samples with large equal-sized quartz, plagioclase and hornblende porphyroclasts,

grains were measured for the rotation analysis. The vorticity data is shown in Figure (6).

In the diagrams shown in Figure (6), a distinction can be made between measurements of relatively low aspect ratio that scatter across a wide range of orientations and those with higher aspect ratio, which have a more restricted range of orientations. The critical values for Rc in investigated samples range from ~2.6 to ~5.4 (Table 2). These values are interpreted as the critical values for Rc separating porphyroclasts that rotated freely from those which have attained a stable position during deformation. Accordingly, Wm ranges from 0.60 to 0.90 (Table 2). The different type of rocks in Tanumaharea typically have feldspar porphyroclasts with aspect ratios of 2 -11 in XZ sections. Low aspect ratio for some samples is inclined at angles close to 45° to the mylonitic foliation and others are densely packed. With increasing aspect ratio, the angle of inclination decreases (Fig. 6). These values of aspect ratio are in harmony with flattening strains and also indicate vertical shortening normal to the main-phase foliation in the gneisses rocks.

6–Discussion

The Ad Damm fault zone is a well-developed NE-trending dextral strike-slip shear zone between the Jiddah and Asir terranes (Johnson et al., 2011). It deforms the Nimas batholith granite of inferred Ediacaran age creating mylonitic granite gneiss with very prominent rotated feldspar porphyroclasts. Fleck and Hadley (1982) suggest an age of approximately 620 Ma for the granite, which implies <620 Ma movement on the fault. Because of this age, Davies (1984) treats the fault as a conjugate dextral shear zone in the Najd system. In the Asir, the shear zones are mostly conformable with the dominant N–S trend of bedding and fold axes, and divide the terranes into discrete structural blocks (Greenwood et al. 1982).

Furthermore, Johnson et al. (2011) show that some are serpentinite decorated and possibly originated during the early to middle Cryogenian as sutures between crustal units within the Asir terrane, but were reactivated during the late Cryogenian to Ediacaran contemporaneously with the final convergence of eastern and western Gondwana and long after peak orogeny in the Asir terrane (680– 649 Ma).

Kassem (2014b) explain that the obtained data show oblate strain symmetry (flattening strain) in the mylonitic granite and metavolcano-sedimentary rocks of the Tanumah area (Table 2). This indicates that the time of deformation represents the accumulation of ductile to brittle deformation during thrusting and intrusions of the mylonitic granitic (diorite suite). This deformation was not by simple shear but it involved vertical shortening produced by a component of pure shear. Pure shear-related vertical shortening caused the subhorizontal foliation in Tanumah area. Pure and simple shear components have a non-linear relationship and make equal contributions to the overall deformation at Wm = 0.71 (Law et al., 2004). Using the fabric skeleton of quartz c-axis fabrics and the maximum strain ratio suggests average kinematic vorticity numbers of 0.5–0.6. These values indicate 60% pure shear component (for relationships see Law et al. 2004), which thus dominates the ductile nappe-emplacement-related deformation.

Kassem and Ring (2004) suggests that subhorizontal foliation by simple shear nappe stacking alone appears to be an unreasonable alternative, since it demands very high shear strains of the order of >10. Also, the rotation of elongate crystals into a subhorizontal position would lead to strain ellipses with aspect ratios of ~100 throughout the entire thickness of the nappes. Such high strains of ≈100 have never been reported in this work. Kassem and Ring (2004) envisage that nappe imbrication associated with a component of pure shear flattening is a general process causing flat-lying

foliations. The rotation of objects by pure shear is faster than in simple shear and thus makes a pure shear component of deformation more likely for producing subhorizontal foliations across nappes. Kassem (2014b) show that mylonitic granite and metavolcano-sedimentary rocks of the Tanumah area are associated with or followed by flattening strain that might be a general process causing flat-lying foliations. The metavolcano-sedimentary and mylonitic granite rocks are intruded by tonalite and granodiorite and granite rocks. The finite strain data indicates that the different type of rocks, such as metavolcanics, meta-andesite, metasedimentary, biotite quartz diorite, gneissic quartz diorite, tonolite and granodiorite and granite rocks were foliated at WNW-ESE trending in the Tanumah area (Fig. 4).

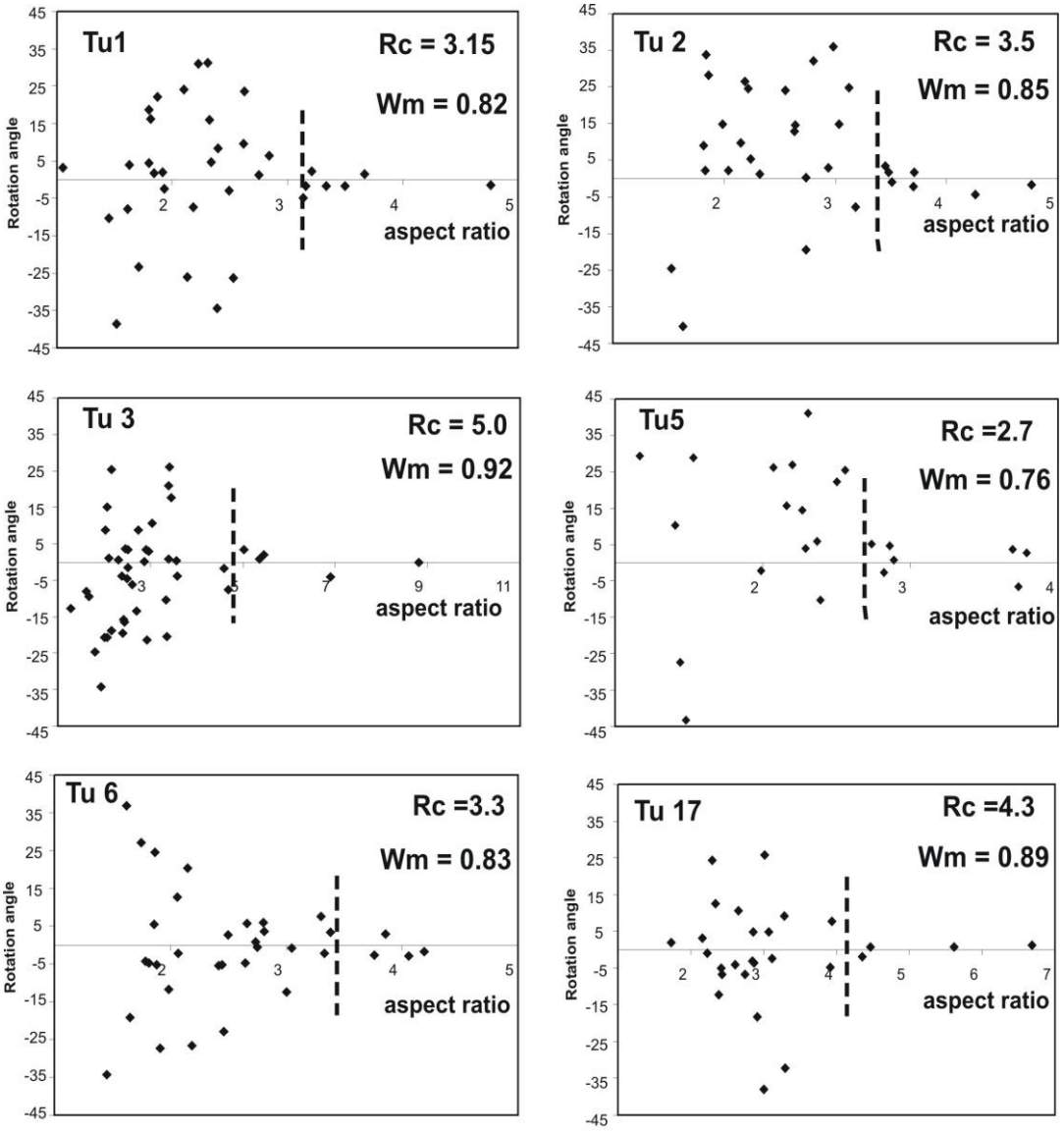

Figure 6) Passchier plot method; Porphyroclast analyses of feldspar grains in XZ sections of rocks; dashed line separates measurements showing wide scatter from those showing stable orientation parallel to foliation; average value of RC for each sample is given in upper left.

(Kassem, 2014b)shows that the kinematic analysis and deformation history areidentified multiple episodes of deformation in the region. Volesky et al. (2003) explain thatthe earliest, D1, episode is marked by E–W compression and the development of S0/S1 schistosity together with N-trending folds and mineral lineation. The D2 episode was caused by transpressional deformation and resulted in the development of the brittle–ductile deformation.

D3 deformation comprises easterly trending, brittle, conjugate faults reflecting SE–NW shortening. D2 and D3 shearing postdated the early Cryogenian arc rocks (Volesky et al., 2003). The minimum age of shearing is determined by plutons of relatively undeformed biotite monzogranite and granite that intrude the sheared rocks.

The observation shows that deformation in the Tanumah area for mylonitic granite and metavolcano-sedimentary rocks of is, in general, distinctly non-coaxial with a dominant top to the west sense of shear suggests that the deformation in the nappe is related to shear coupling on the thrusts which bound the Tanumah area (Kassem, 2014b). Therefore, it seems plausible to assume that the main deformation events are also interpreted to have formed during thrusting which formed the summit of Tanumah area. In addition, they wrapped in a roughly north–south orientation. In this case, stretching lineations during thrusting trend W/WNW and associated kinematic indicators record top to the west tectonic transport.This conclusion supports the study by (Johnson et al., 2011).

7–Conclusions

The kinematic vorticity number for the gneisses rocks from exposed in the Tanumah area ranges from ~0.6-0.9, and together with the strain data suggest deviations from simple shear. It can be concluded that nappe stacking occurred early during the thrusting event, probably by brittle imbrication and that ductile strain was superimposed on the nappe structure at high-pressure. The accumulation of ductile strain during overthruting was not purely by simple shear. It involved a component of vertical shortening, which caused the subhorizontal foliation in the Tanumah area and environs, which is subparallel to the tectonic contacts with the under- and overlying nappes. In most cases, this foliation formed during thrusting of the nappes onto each other suggesting that nappe stacking was associated with vertical shortening. This observation contrasts with the widely held opinion that nappe formation in orogens is by simple-shear deformation.

Acknowledgments:

The authors would like to extend their sincere appreciation to the Deanship of Scientific Research at King Saud University for its funding of this research through the Research Group project no RGP-VPP-230.The author would like to thank Prof. U. Zaineldeen andDr. S. Lotfifor their appreciate comments which help him to improve manuscript.

References:

Al-Saleh, A.M., Kassem, O. M. K. 2012. Microstructural, Strain Analysis and $^{40}Ar/^{39}Ar$ Evidence for the Origin of the Mizil Gneiss Dome, Eastern Arabian Shield, Saudi Arabia. Journal of African Earth Science: 70, 24–35.

Cowan, D. S. 1990. Kinematic analysis of shears zones in sandstone and mudstone of the Shimanto belt, Shikokn, SW Japan. Journal of Structural Geology: 12, 431–441.

Davies, F.B. 1984. Strain analysis of wrench faults and collision tectonics of the Arabian–Nubian Shield. Journal of Geology: 82, 37–53.

Doebrich, J. L. Al-Jehani, A. M., Siddiqui, A. A., Hayes, T. S., Saleh, Y., Wooden, J. L., Johnson, P. R., Kattan, F. H., Shaikan, B., Basahel, M., Zahran, H., Al-Shammari, A. 2007. Geology and Mineral Resources of the Ar Rayn Terrane, Eastern Arabian Shield, Kingdom of Saudi Arabia, Precambrian Research: 158, 17–50.

Elliott, D. 1972. Deformation paths in structural geology. Bulletin of the Geological Society of America: 83, 2621–2638.

Fleck, R. J., Hadley, D. G. 1982. Ages and Strontium Initial Ratios of Plutonic Rocks in a Transect of the Arabian Shield. Saudi Arabian Deputy Ministry for Mineral Resources Open-File Report USGS-OF-03–38, 43 p.

Fleck, R.J., Greenwood, W.R., Hadley, D.G., Anderson, R.E., Schmidt, D.L. 1980.

Rubidium-strontium geochronology and plate-tectonic evolution of the southern part of the Arabian shield: U.S. Geological Survey Professional Paper 1131, 37 p.

Flinn, D., 1962. On folding during three-dimensional progressive deformation. Quarternary Journal of Geological Society of London: 118, 385–433.

Fry, N. 1979. Random point distributions and strain measurement in rocks. Tectonophysics: 60, 89–105.

Genna, A., Nehlig, P., Le Goff, E., Guetrrot, C., Shanti, M. 2002. Proterozoic tectonism of the Arabian Shield. Precambrian Research: 117, 21–40.

Ghosh, S. K., Ramberg, H. 1976. Reorientation of inclusions by combination of pure shear and simple shear. Tectonophysics: 34, 1–70.

Greenwood, W. R. 1979. Geologic map of the An Nimas quadrangle, sheet 19/42C, Kingdom of Saudi Arabia, with a section on Economic mineral deposits, by R. J. Roberts, and a section on Aeromagnetic studies by G. E. Andreasen: Saudi Arabian Directorate General of Mineral Resources Geologic Map GM-37,scal 1:100,000; text, 33p.

Greenwood, W.R., Stoeser, D.B., Fleck, R.J., Stacey, J.S.1982. Late Proterozoic island-arc complexes and tectonic belts in the southern part of the Arabian shield, Kingdom of Saudi Arabia: Saudi Arabian Deputy Ministry for Mineral Resources Open-File Report USGS-OF-02–8, 46 p.

Hargrove, U. S. 2006. Crustal Evolution of the Neoproterozoic Bi'r Umq Suture Zone, Kingdom of Saudi Arabia, Geochronological, Isotopic, and Geochemical Constraints, Ph.D. Thesis, University of Texas at Dallas, pp. 343.

Jeffery, G. B. 1922. The motion of ellipsoidal particles immersed in a viscous fluid. Proceedings Royal Society London Series A: 102, 161–179.

Johnson, P. R., Andresen, A., Collins, A.S., Fowler, A. R., Fritz, H., Ghebreab, W., Kusky, T., Stern, R. J. 2011. Late Cryogenian–Ediacaran history of the Arabian–Nubian Shield: A review of depositional, plutonic, structural, and tectonic events in the closing stages of the northern East African Orogen. Journal of African Earth Sciences: 61, 167–232.

Johnson, P. R., Woldehaimanot, B. 2003. Development of the Arabian–Nubian Shield, Perspectives on Accretion and Deformation in the Northern East African Orogen and the Assembly of Gondwana", in Proterozoic East Gondwana, Supercontinent Assembly and Breakup, ed. M. Yoshida, B. F. Windley, and S. Dasgupta. Geological Society of London Special Publications 206, pp. 289–325.

Kassem, O.M. K., Abd El Rahim S. H., El Nashar E. R. 2012. Strain analysis and Microstructural evolution characteristic of Neoproterozoic rocks associations of Wadi El Falek, Centre Eastern Desert, Egypt. Geotectonics: 46, 379–388.

Kassem, O. M. K. 2008. Strain analysis and heterogeneous deformation in the Migif area, Eastern Desert, Egypt, Annals Geological Survey: 30, 103–119.

Kassem, O. M. K. 2011. Determining Heterogeneous deformation for Granitic rocks in the Northern thrust in Wadi Mubark belt, Eastern Desert, Egypt. Geotectonics Journal:45, 244–254.

Kassem, O. M. K. 2012. Kinematic Vorticity Technique for Porphyroclasts in the Metamorphic Rocks: An Example from the Northern thrust in Wadi Mubarak belt, Eastern Desert, Egypt. Arabian Journal of Geosciences, 5, 159–167.

Kassem, O. M. K. 2014a. Kinematic analysis of the Migif area in the Eastern Desert of Egypt. Journal of African Earth Science: 90, 136–149.

Kassem, O. M. K. 2014b. Strain analysis and deformation in the Tanumah Area, Arabian Shield, Saudi Arabia, Arabian Journal of Geosciences: Doi 10.1007/s12517-014-1397-8.

Kassem, O. M. K., Ring, U. 2004. Underplating-related finite-strain patterns in the Gran Paradiso massif, Western Alps, Italy: heterogeneous ductile strain superimposed on a nappe stack. Journal of the Geological Society, London: 161, 875–884.

Kassem, O. M.K., Abdel Raheim, S. 2010. Finite strain analysis for the Metavolcanic-sedimentary rocks in the Gabel El- Mayet region, Central Eastern Desert, Egypt. Journal of African Earth Science: 58, 321–330.

Law, R.D., Searle, M.P., Simpson, R.L. 2004. Strain, deformation temperatures and velocitiy of flow at the top of the Greater Himalayan Slab, Everest Massif, Tibet. Journal of the Geological Society, London: 161, 305–320.

Lister, G. S., Williams, P. F. 1983. The partitioning of deformation in flowing rock masses. Tectonophysics: 92, 1–33.

Malvern, L. E. 1969. Introduction to the Mechanics of a continuous medium. Prentice-Hall, Englewood Cliffs, New Jersey.

Means, W. D., Hobbs, B. E., Lister, G. S., Williams, P. F. 1980. Vorticity and non-coaxiality in progressive deformations. Journal of Structural Geology: 2, 371–378.

Nehlig, P., Genna, A., Asfirane, F. 2002. A review of the Pan-African evolution of the Arabian Shield: GeoArabia: 7, 103–124.

Passchier, C.W. 1986. Flow in natural shear zones-the consequences of spinning flow regimes. Earth and planetary Science Letters: 77, 70–80.

Passchier, C.W. 1987. Stable positions of rigid objects in non-coaxial flow-a study in vorticity analysis. Journal of Structural Geology: 9, 679–690.

Passchier, C. S., Urai, J. L. 1988. Vorticity and strain analysis using Mohr diagrams. Journal of Structural Geology: 10, 755–763.

Passchier, C.W. 1990. Reconstruction of deformation and flow parameters from deformed vein sets. Tectonophysics: 180, 185–199.

Peach, C. J., Lisle, R. J. 1979. A fortran IV program for the analysis of tectonic strain using deformed elliptical markers. Computer and Geoscience: 5, 325–334.

Prinz, W. C. 1975. Reconnaissance geology of the Jabal Aya quadrangle, sheet 18/42 A, Kingdom of Saudi Arabia, with a section on Aeromagnetic studies, by G. E. Andreasen: Saudi Arabian Directorate General of Mineral Resources Geologic Map GM-17,scal 1:100,000; text, 9p.

Ramsay, J. G., Huber, M. I. 1983. The Techniques of Modern Structural Geology, vol. 1. Academic Press, London.

Ring, U. 1998. Exhumation of blue schists from Samos Island. Geological Society of Greece Bulletin V. 32, pp. 97–104.

Ring, U., Brandon, M.T. 1999. Deformation and mass loss in the Franciscan subduction complex: Implications for exhumation processes in accretionary wedges, in Exhumation processes: Normal Faulting, Ductile Flow, and Erosion, edited by Ring, U., Brandon, M.T., Lister, G.S., Willett, S.D., Geological Society of London Special Publications: 154, 55–86.

Ring, U., Brandon, M.T., Ramthun, A. 2001. Solution-mass-transfer deformation adjacent to the Glarus thrust, with implications for the tectonic evolution of the Alpine wedge in eastern Switzerland. Journal of Structural Geology: 23, 1491–1505.

Ring, U., Kassem, O. M. K. 2007. The nappe rule: why does it work? Journal of the Geological Society: 164, 1109–1112.

Simpson, C., De Paor, D.G. 1997. Practical analysis of general shear zones using the porphyroclast hyperbolic distribution method: an example from the Scandinavian Caledonides. In: Sengupta, S., (Ed.), Evolution of Geological Structures in Micro- to Macro- Scales, Chapman and Hall, pp. 169–184.

Simpson, C., De Poar, D. G. 1993. Strain and Kinematic analysis in general shear zones. Journal of Structural Geology: 15, 1–20.

Stern, R. J. 1994. Arc Assembly and Continental Collision in the Neoproterozoic East African Orogen, Implications for the Consolidation of Gondwanaland", Annual Review of Earth Sciences: 22, 319–351.

Stoeser, D. B., Stacey, J. S., Greenwood, W. R., Fischer, L. B. 1984. U/Pb Zircon Geochronology of the Southern Part of the Nabitah Mobile Belt and Pan-African Continental Collision in the Saudi Arabian Shield", Saudi Arabian Deputy Ministry for Mineral Resources Technical Record USGS-TR-04-5, pp. 88.

Stoeser, D. B., Stacey, J. S. 1988. Evolution, U-Pb geochronology, and isotope geology of the Pan-African Nabitah orogenic belt of the Saudi Arabian shield, in S. El-Gaby and R.O. Greiling, eds., The Pan-African Belt of Northeast Africa and Adjacent Areas: Braunschweig/ Wiesbaden, Vieweg and Sohn, p. 227–288.

Stoeser, D. B., Frost, C. D.2006. Nb, Pb, Sr, and O Isotopic Characterization of Saudi Arabian

Shield Terranes. Chemical Geology: 226, 163–188.

Stoeser, D.B., Camp, V.E. 1985. Pan-African microplate accretion of the Arabian Shield. Geological Society of America Bulletin: 96, 817–826.

Tikoff, B., Teyssier, C. 1994. Strain and fabric analyses based on porphyroclast interaction. Journal of Structural Geology: 16, 477–491.

Volesky, J. C., Stern, R. J. , Johnson, P. R. 2003. Geological control of massive sulfide mineralization in the Neoproterozoic Wadi Bidah shear zone, southwestern Saudi Arabia, inferences from orbital remote sensing and field studies.Precambrian Research: 123, 235–247.

Wallis, S. R. 1992. Vorticity analysis in a metachert from the San-bagawa Belt, SW Japan. Journal of Structural Geology: 14, 271–280.